Article

Optimized TiO₂ Coatings on AISI 316 Steel for Advanced Photocatalytic Wastewater Treatment: Mechanism and Performance

Maria-Anthoniette Oghenetejiro Onoriode-Afunezie,* Povilas Urbanskis, Inga Urniežaitė, and Agnė Šulčiūtė

Cite This: ACS Omega 2025, 10, 34666−34682

Read Online

ACCESS | Metrics & More | Article Recommendations

ABSTRACT: The development of robust and efficient photocatalysts is essential for sustainable wastewater treatment. This study evaluates the photocatalytic degradation of ciprofloxacin (CIP) using three TiO₂-coated systems: TiO₂ nanotube arrays (TiO₂ NTA), Bare-Coated TiO₂, and Methanol-Enhanced TiO₂, with a focus on coating uniformity, interfacial stability, and reaction pathways. Surface morphology analysis (SEM) revealed that TiO₂ NTA exhibited a uniform surface, optimizing active site exposure and photocatalytic efficiency. Methanol-Enhanced TiO₂ formed a refined crack pattern, enhancing coating stability and facilitating uniform distribution of TiO₂ particles, while Bare-Coated TiO₂ showed a highly fractured surface, limiting its catalytic efficiency. X-ray diffraction (XRD) confirmed that the anatase phase was the dominant crystalline structure across all coatings, ensuring photocatalytic activity.

High-performance liquid chromatography−mass spectrometry (HPLC-MS) analysis revealed distinct degradation patterns, with TiO₂ NTA facilitating rapid fragmentation of CIP into multiple low m/z intermediates, indicating aggressive oxidative breakdown. Methanol-Enhanced TiO₂ exhibited a more controlled degradation pathway, with prominent peaks at 316 (+) m/z and 285 (+) m/z, suggesting selective oxidation and gradual mineralization rather than immediate fragmentation. The degradation mechanism of Methanol-Enhanced TiO₂ likely favored sustained transformation steps, potentially reducing the accumulation of harmful byproducts. Under ultraviolet (UV)-driven photocatalysis, Methanol-Enhanced TiO₂ outperformed Bare-Coated TiO₂, achieving accelerated degradation kinetics, while TiO₂ NTA maintained high stability but lagged in mineralization efficiency. The introduction of ozone further enhanced degradation, ensuring complete CIP removal across all systems. Methanol-Enhanced TiO₂ maintained a degradation efficiency of 88.72% after five reuse cycles, closely matching the 88.75% TiO₂ NTA, demonstrating strong reusability and potential for scalable wastewater treatment applications in photocatalytic treatment reactors. These findings underscore the importance of coating methodologies and interfacial properties in optimizing TiO₂-based photocatalysts, positioning Methanol-Enhanced TiO₂ as a viable and durable alternative to TiO₂ NTA for sustainable micropollutant removal.
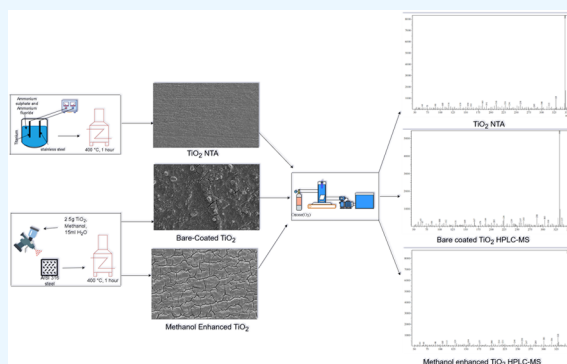
1. INTRODUCTION

The increasing complexity of micropollutants and the harsh environments encountered in wastewater treatment systems underscore the critical need for advanced materials in the final stages of treatment.[1] Advanced materials, including nanomaterials and hybrid composites, exhibit unique physicochemical properties that significantly improve micropollutant removal and offer resistance to chemical degradation and corrosion, thus extending the operational lifespan of treatment systems.[2,3] These materials improve adsorption, catalytic degradation, and corrosion resistance, contributing to more efficient and sustainable wastewater treatment processes.[4] Among these, titanium dioxide (TiO₂) has garnered significant attention for its photocatalytic properties which are capable of degrading a wide range of organic pollutants under ultraviolet (UV) and, with appropriate doping, in visible light.[5−7]

Modifications to TiO₂ surfaces, including coupling with carbon-based materials such as graphene oxide, have improved its photocatalytic efficiency and broadened its applicability beyond traditional UV-driven reactions.[7,8] This makes TiO₂ a versatile and promising candidate for wastewater treatment applications, especially to remove persistent pollutants such as pharmaceuticals and industrial dyes.[9]

In addition to photocatalytic activity, the stability and longevity of these materials in real-world wastewater environ-

ments are critical. Corrosion and mechanical degradation often limit the operational lifespan of treatment components, affecting cost-effectiveness and system reliability.[10,11] Stainless steel, particularly AISI 316, is commonly used in industrial wastewater treatment due to its excellent corrosion resistance, mechanical strength, and compatibility with various coatings.[12] When TiO_2 is applied to AISI 316 substrates, it increases steel durability while improving pollutant degradation through photocatalysis.[13,14] Surface modification techniques such as plasma treatment and spray coating have been developed to improve TiO_2 adhesion and uniformity on stainless steel, which is crucial to maintain photocatalytic efficiency over time.[15,16] These hybrid systems show great potential to create robust multifunctional wastewater treatment technologies that can withstand aggressive chemical and physical conditions.

Despite the promise of TiO_2-coated AISI 316 steel, the effects of wastewater constituents on coating stability require further investigation.[17] Organic solvents such as methanol, often present in industrial effluents or used as additives during treatment, can affect the chemical and mechanical integrity of TiO_2 layers.[17,18] The interaction of methanol with the coating surface may influence adhesion strength, photocatalytic activity, and resistance to fouling or degradation. Understanding the design and regulatory mechanisms is essential to design coatings that maintain performance under realistic operational conditions. Few studies have addressed this interaction, leaving a significant knowledge gap in the field. This gap poses a barrier to the implementation of TiO_2-coated stainless steel on a large scale in various wastewater treatment applications.

Advanced photocatalytic materials, including nanobiohybrids and carbon nanomaterials such as carbon nanotubes (CNTs) and carbon nanofibers (CNFs), complement the capabilities of TiO_2 by offering improved adsorption and catalytic properties.[19] These materials can effectively adsorb heavy metals and organic contaminants and can be integrated with TiO_2 coatings to further improve treatment performance.[19,20] Furthermore, plasmonic photocatalysts and conjugated microporous polymers (CMPs) have demonstrated efficiency in degrading complex pesticides and pharmaceuticals, showcasing the broad potential of hybrid advanced materials in environmental remediation.[21,22] Such materials often feature energy-efficient synthesis methods and can be incorporated into existing systems cost-effectively, supporting sustainable wastewater treatment development.[4,21] However, integrating these diverse materials with robust substrates such as AISI 316 steel remains an area for further exploration. The stability of these composite coatings in chemically complex and variable wastewater streams is an ongoing challenge.

The method of application of TiO_2 coatings plays a crucial role in determining their uniformity, thickness, and durability. Spray coating has emerged as an environmentally friendly, precise technique that minimizes material waste while ensuring uniform coverage on stainless steel substrates.[16,23] Optimizing the thickness of the TiO_2 layers balances photocatalytic efficiency with mechanical resistance, where thinner layers enhance light penetration, and thicker layers improve wear resistance.[24,25] Furthermore, doping TiO_2 with nanomaterials and applying advanced coating techniques, such as sol–gel and electrospinning, have shown promise in improving photocatalytic activity and coating adherence.[13,26,27] Such innovations also enable multifunctional coatings with antimicrobial properties, which are valuable in wastewater settings prone to

microbial contamination.[28] These developments highlight the importance of coating technology in the advancement of durable and efficient wastewater treatment materials.

Integration of TiO_2-coated AISI 316 steel with electrochemical processes further enhances pollutant degradation by facilitating the generation of reactive species such as hydroxyl radicals.[29,30] This combination broadens the operational conditions under which photocatalytic degradation is effective, including variable pH and temperature range.[8] It also helps to address the removal of persistent contaminants such as ciprofloxacin, a common antibiotic-resistant to conventional treatments.[31−33] By improving both photocatalytic and electrochemical degradation pathways, such systems offer a robust solution for complex industrial effluents. These advances align with increasing environmental regulations that require higher water quality and more sustainable treatment technologies.[34] Continued research is needed to optimize these integrated approaches, especially considering coating stability in the presence of solvents such as methanol.

This study addresses these critical gaps by developing a sustainable TiO_2-coated AISI 316 stainless steel system, focusing on the impact of methanol on the stability of the coating and photocatalytic performance. Using precise spray-coating techniques, it aims to optimize TiO_2 layer properties for durability and pollutant removal efficiency under realistic wastewater conditions. The research highlights the unique advantages of combining corrosion-resistant stainless steel with advanced photocatalytic materials to extend the useful life of the equipment and reduce operational costs. It also explores the regulatory mechanisms by which methanol influences coating behavior, an understudied area crucial for practical deployment. Ultimately, this work advances the development of multifunctional materials designed for sustainable, efficient, and resilient wastewater treatment, meeting current environmental and industrial challenges.

2. MATERIALS AND METHODS

2.1. Experimental Solutions and Model Compounds.
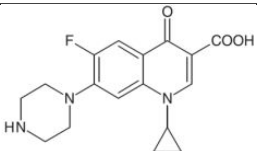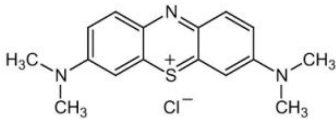The following materials (Table 1) were used for the cleaning

Table 1. Materials and Compounds Used for Catalyst Synthesis

chemical substance	chemical formula	country of origin
acetone, 99.8% analytically pure	CH_3COCH_3	Eurochemicals, Lithuania
2-propanol, 99.7% analytically pure	$(CH_3)_2CHOH$	Eurochemicals, Lithuania
ammonium fluoride, 98% analytically pure	NH_4F	Sigma-aldrich, Germany
ammonium sulfate, 99.0% analytically pure	$(NH_4)_2SO_4$	Sigma-aldrich, Germany
methanol, ≥99% analytically pure	CH_3OH	eurochemicals, Lithuania

and synthesis of AISI 316 steel and titanium dioxide nanotube arrays (NTA): acetone, 2-propanol, ammonium fluoride (NH_4F), and ammonium sulfate ($(NH_4)_2SO_4$).

2.2. Synthesis and Characterization of TiO_2 Photocatalysts. 2.2.1. Synthesis of a TiO_2 Nanotube Array (NTA).
Cleaning of titanium metal was performed using acetone and 2-propanol before the electrophoresis process. For this deposition, electrolyte solutions were prepared by dissolving 5.5 g/L NH_4F and 132 g/L $(NH_4)_2SO_4$ in first-grade

Table 2. Properties and Chemical Structures of Ciprofloxacin and Methylene Blue

Characteristics	Ciprofloxacin hydrochloride	Methylene Blue
Molecular structure		
CAS Nr.	86393320	61-73-4
IUPAC name	1-cyclopropyl-6-fluoro-4-oxo-7-piperazin-1-ylquinoline-3-carboxylic acid	[7-(dimethylamine) phenothiazin-3-ylidene]- dimethylazanium; chloride
Molecular Formula	$C_{17}H_{18}FN_3O_3$	$C_{16}H_{18}ClN_3S$
Molecular Weight	331.34	319.19
Log K^{now}	0.28	0.75
Solubility in water	36 mg/L at 25 °C	43.6 mg/L at 25 °C

demineralized water. The surface of the NTA was roughened with 200-grit sandpaper and smoothed with 800-grit sandpaper. A glass tube served as a reactor during the electrophoretic deposition of TiO_2 NTA. The synthesized TiO_2 NTA was calcinated in an oven at 400 °C for 1 h.[35] The EPD was carried out at a constant potential of 20 V for 2 h. The optimal calcination temperature of 400 °C for TiO_2 NTA is mainly due to the balance achieved between crystallinity,[36] phase composition,[37] and photocatalytic efficiency.[37][38]

2.2.2. Synthesis of TiO₂ Coatings. AISI 316 steel plates underwent a series of preparatory procedures, including cutting, sanding, and thorough cleaning with water, acetone, 2-propanol, and deionized water. Subsequently, 2.5 g of TiO_2 nanoparticles (Degussa P25), 15 mL of deionized water, along varying volumes of methanol (ranging from 0.5 to 6.0 mL), were aerosolized on steel plates using a spray gun apparatus. Plates prepared without methanol were designated as Bare-Coated TiO_2, while those prepared with 1.5 mL of methanol were referred to as Methanol-Enhanced TiO_2. The use of methanol concentrations ranging from 0.5 to 6.0 mL in TiO_2 synthesis is mainly due to its role in improving reaction kinetics,[39] improving material properties,[40] and influencing photocatalytic performance.[41] Methanol acts as a solvent and reactant, affecting the deposition and crystallization processes of TiO_2, which are crucial for achieving the desired characteristics and efficiency of the material in applications such as photocatalysis. The resulting coated plates were subjected to a calcination process at a temperature of 400 °C for 1 h.

2.2.3. TiO₂ Dispersion and Concentration Analysis. To determine the relationship between methanol volume and TiO_2 concentration, the Beer–Lambert Law (eq 1) was applied, where absorbance (A) is proportional to the concentration (c), path length (l), and molar absorptivity (ε)[39]

$$A = \varepsilon cl \tag{1}$$

Absorbance measurements were obtained using a ultraviolet–visible (UV–vis) spectrophotometer at a fixed wavelength corresponding to TiO_2 nanoparticle absorption of 325 nm. A series of TiO_2 suspensions were prepared by dispersing

2.5 g of TiO_2 in varying methanol volumes (0.5, 1.0, 1.5, 3.0, 4.5, and 6.0 mL), ensuring uniform mixing before measurement. The resulting absorbance values were used to calculate TiO_2 concentrations in mol/L.

2.2.4. Catalyst Morphology and Elemental Analysis. A Quanta 200 FEG electron microscope (FEI Company, The Netherlands) was used for scanning electron microscopy (SEM). A secondary electron detector with a 10−20 kV accelerating voltage was used for a high-resolution image preparation (resolution not <3 nm) at a working distance of 7.5−10 nm. The observation of the sample surface was performed in a high vacuum regime ($\leq 1.5 \times 10^{-3}$ Pa) using a life-fiber detector (LFD).

X-ray energy dispersive spectroscopic analysis (EDS) was also performed using a scanning electron microscope with an X-ray dispersion spectrometer Flash 4030 (Bruker, Germany) built into it.

2.2.5. Crystallographic Structure of TiO₂. The crystal structure of the samples was identified using an X-ray diffractometer (Bruker D8 Discovery) that worked in the theta−theta configuration. The main parameters of the XRD configuration theta−theta were Cu Kα radiation ($\lambda = 0.15406$ nm, K_β suppressed by the Ni filter); 500 mm goniometer, step size of 0.02° step size, 20−70° scan range; 0.3° fixed div slit and linear Lynx eye PSD detector. Analysis of the obtained XRD patterns was performed using the PDF-4 database, ICDD Card No 03−065−3362 (International Center for Diffraction Data, ICDD).

The crystallite size of the TiO_2 samples was determined using the Scherrer equation[40] (eq 2), which provides an estimation based on the broadening of diffraction peaks in the X-ray diffraction (XRD) pattern. The equation is given as

$$D = \frac{K\lambda}{\beta \cos \theta} \tag{2}$$

where D is the crystallite size, K is the Scherrer constant (typically 0.94 for spherical particles), λ is the wavelength of the Cu Kα radiation (0.154 nm), β is the full width at half-maximum (fwhm) of the most intense diffraction peak (in

radians), θ is the Bragg angle (half of the corresponding 2θ value).

For this study, the most prominent anatase peak was selected for the calculation of the crystallite size of TiO_2 catalysts while the fwhm values were extracted from the XRD patterns, and the Scherrer equation was applied to estimate the average crystallite size of Methanol-Enhanced TiO_2, Bare-Coated TiO_2, and TiO_2 NTA. This method allowed us to compare the structural properties of the coatings, revealing variations in crystallite sizes that can influence photocatalytic performance.

2.3. Pollutant Degradation Study. *2.3.1. Model Compounds and Experimental Solutions.* The chemicals used for this experiment, namely ciprofloxacin (CIP) and methylene blue (MB), were prepared from analytical grade (>99% purity) chemicals and purchased from TCI America. Methylene blue is widely used to assess photocatalytic degradation due to its well-defined absorption peak,[41] stability,[42] representative nature as an organic pollutant,[43] strong interaction with catalysts,[44] distinct color change upon degradation,[45] and ease of handling for quantitative analysis.[41] All Ciprofloxacin and methylene blue solutions were prepared with first-grade demineralized water as the solvent. Table 2 contains the properties and chemical structures of both ciprofloxacin and methylene blue.

2.3.2. Photocatalytic Degradation of Methylene Blue (MB). To evaluate the photocatalytic efficiency of TiO_2 coatings on AISI 316 steel and TiO_2 NTA, the degradation of methylene blue (MB) was used as a model reaction. MB solutions were prepared at a concentration of 10 mg/L and exposed to UV irradiation with an irradiation intensity of 3.2 mW/cm^2 using an Aqua Forte 9 W UV−C lamp, a professional water product manufactured by SIBO Fluidra, Netherlands in the presence of each TiO_2-coated sample. The concentration of MB was monitored at a wavelength of 665 nm using the UV−vis spectrophotometer "Spectronic GENESYS 8" from Thermo Scientific at set time intervals. Reaction kinetics were evaluated by plotting the change in MB concentration over time, allowing a comparative analysis of degradation rates on the different TiO_2-coated surfaces.

2.3.3. Adsorption on Catalyst. For the ciprofloxacin (CIP) wastewater degradation study, the adsorption characteristics were initially evaluated under dark conditions. Both TiO_2-coated AISI 316 steel and TiO_2 NTA were immersed in CIP solutions with a starting concentration of 1 mg/L. The initial CIP concentration of 1 mg/L used in the adsorption study was selected to reflect the higher concentrations occasionally reported in hospital and pharmaceutical wastewater, which typically range from nanograms per liter (ng/L) to low milligrams per liter (mg/L) levels.[46,47] This choice ensures observable photocatalytic activity within a controlled laboratory setting while maintaining relevance to real wastewater treatment scenarios. The samples were kept in the dark for 30 min to ensure equilibrium adsorption. Periodic sampling allowed the measurement of residual CIP concentrations by UV−vis spectrophotometry at 277 nm, establishing the adsorption capacity and preparing the samples for subsequent photocatalytic tests.

2.3.4. Photocatalytic Degradation of Ciprofloxacin (CIP). After the adsorption phase, both photocatalysis and photocatalytic ozonation degradation of CIP were evaluated (Figure 1). The samples were exposed to ultraviolet (UV) light in the first experiment and then to UV light with ozonation in the
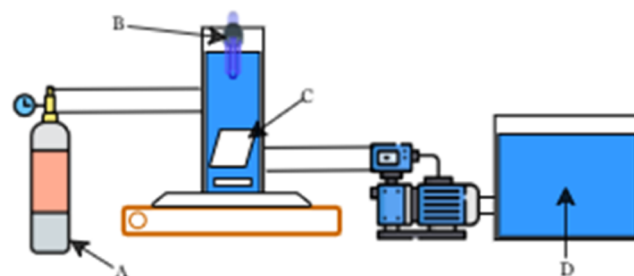
Figure 1. Photocatalytic degradation setup: (a) ozone gas, (b) UV light, (c) TiO_2 catalyst, and (d) ciprofloxacin.

second experiment. UV irradiation was provided by an Aqua Forte 9 W UV−C lamp with an irradiation intensity of 3.2 mW/cm^2, a professional water product manufactured by SIBO Fluidra, Netherlands. CIP concentrations were measured at specified intervals to calculate degradation rates. Ozone gas was introduced into the experimental setup through a 6 mm silicone tubing connected to mini air stone diffusers using Certizon 200 ozone generators from "Sander" in Germany.

Each experiment lasted between 10 and 60 min and UV monitoring of CIP was done at 277 nm using the UV−vis "Spectronic GENESYS 8" spectrophotometer from Thermo Scientific. The samples were extracted from the reactor using a 5 mL medical syringe. Kinetic data was analyzed using a pseudo-first-order kinetic model, providing a quantitative comparison of the photocatalytic performance of the TiO_2-coated substrates.

2.3.5. Reusability and Stability of the TiO_2 NTA Photocatalyst. To explore the reusability and stability of the synthesized TiO_2 NTA and sprayed TiO_2-coated photocatalysts used in this study, cyclic reuse experiments were conducted. Cyclic and reusability experiments in photocatalytic wastewater treatment are essential to evaluate the long-term efficiency, stability, and degradation resistance of photocatalysts, ensuring cost-effective and sustainable water purification. The degradation of CIP was evaluated by monitoring the C/C_0 ratios for the five consecutive runs within the reactor.

2.3.6. Degradation Pathway. To follow the ciprofloxacin (CIP) wastewater degradation pathway, we employed high-performance liquid chromatography−mass spectrometry (HPLC-MS). The mass spectra were collected using an LCMS-2020 (ESI+) (Shimadzu; Japan) system equipped with an ultraviolet detector and coupled to a mass spectrometer. The HPLC utilized a reverse-phase C-Ph column (4.6 mm × 100 mm), which is well-suited for separating polar and nonpolar compounds based on their hydrophobicity.

HPLC separation was achieved using a mobile phase composed of acetonitrile and water +0.1% formic acid, gradient conditions at a flow rate of 0.6 mL/min. The mass spectrometer functioned in positive ionization mode, facilitating the detection of primary molecular ions and characteristic fragments of ciprofloxacin (CIP) and its derivatives across a wide mass spectrum. This configuration enabled thorough monitoring, with CIP being identified at 254 nm for accurate quantification. The combination of HPLC and mass spectrometry presents a robust methodology for the identification of CIP and its degradation products, yielding significant insights into the compound's dynamics and transformation during photodegradation.
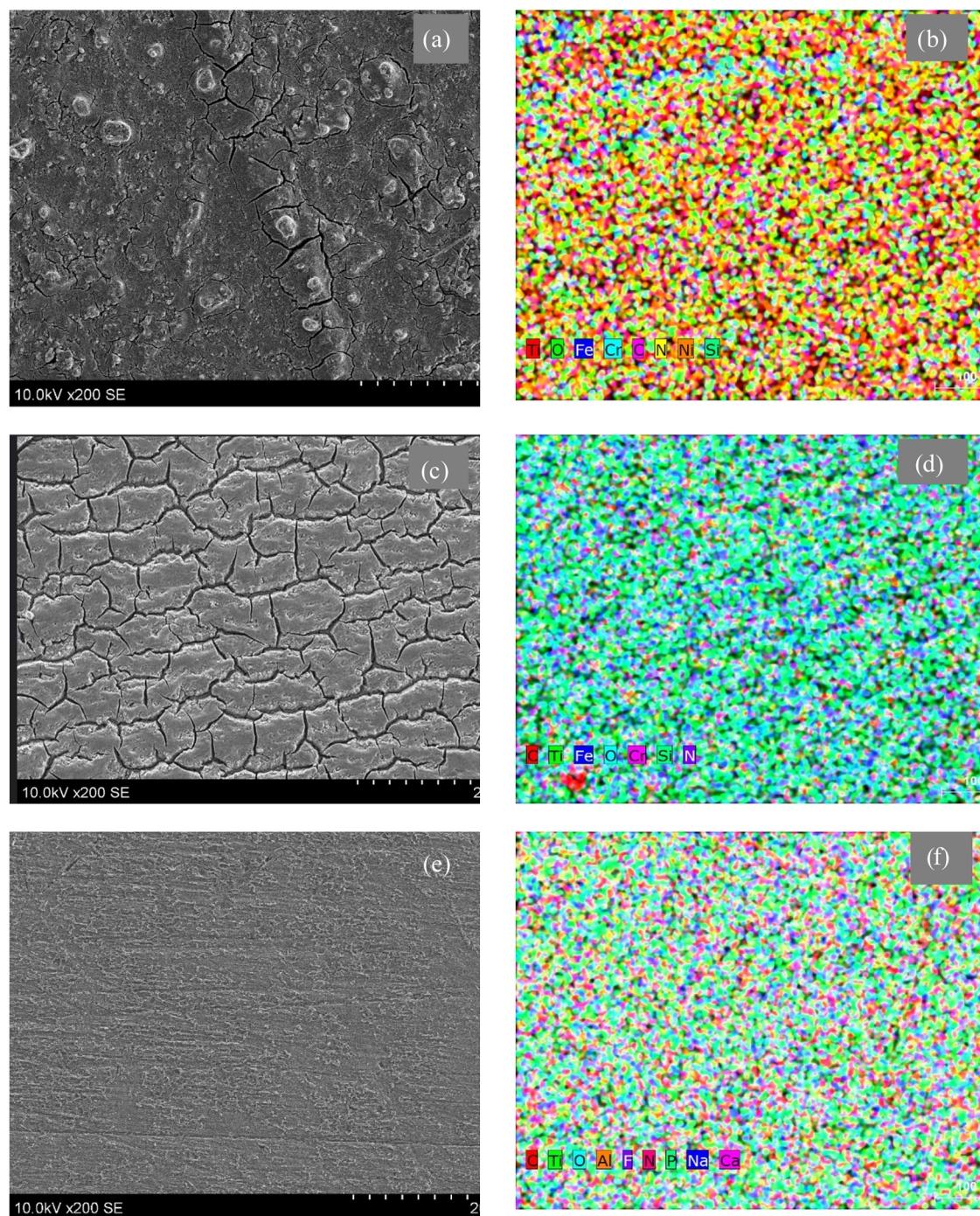
Figure 2. SEM (magnification × 10,000) (a, c, e) and EDS maps (b, d, f) of TiO$_2$-coated samples synthesized at 400 °C.

Samples collected at regular intervals during photocatalytic degradation experiments were analyzed to identify the absence of CIP in the sample. The degradation pathway was reconstructed based on the temporal profiles of these intermediates, offering detailed insights into the mechanisms of CIP breakdown in TiO$_2$-coated AISI 316 steel and TiO$_2$ NTA systems.

3. RESULTS AND DISCUSSION

3.1. Synthesis of TiO$_2$ Photocatalyst. *3.1.1. Surface Morphology.* This section examines the surface morphologies of TiO$_2$ coatings developed using varying methods and methanol concentrations, aiming to correlate structural characteristics with photocatalytic performance. By analyzing the effects of methanol concentration and deposition techniques on the adherence, homogeneity, and structural stability of the TiO$_2$ layers, the role of coating morphology in influencing photocatalytic activity can be better understood.

Figure 2a, which is the Bare-Coated TiO$_2$ shows a highly cracked and uneven surface morphology. The large, defined crack patterns indicate minimal adherence and structural integrity, suggesting that without methanol, the TiO$_2$ particles may not achieve optimal distribution or binding on the steel substrate. This uneven coating might hinder effective photocatalytic activity, as the available active sites could be irregularly dispersed.

In contrast, in Figure 2c, the Methanol-Enhanced TiO$_2$ presents a more refined, tightly packed crack pattern with improved homogeneity across the surface. The addition of 1.5 mL methanol appears to enhance the coating's structural stability and adherence, resulting in a more uniform distribution of TiO$_2$ particles. This even layer potentially maximizes active sites, contributing to its observed superior photocatalytic performance.[17] The smaller, less pronounced cracks reflect a better-controlled drying process and enhanced coating stability,[48] suggesting that the Methanol-Enhanced TiO$_2$ might provide an optimal balance for the spray coating.

Meanwhile, in Figure 2d, the TiO$_2$ NTA sample shows a much smoother and cohesive surface with minimal cracking.[35] This electrophoretic deposition method allows us to achieve a compact and continuous layer of TiO$_2$ on the steel substrate, indicating strong adherence and uniformity. The superior structural integrity aligns with its proven photocatalytic efficiency, as the continuous surface likely maximizes the exposure of active sites without the interruptions seen in the spray-coated samples.

Overall, these observations emphasize the significant influence of methanol concentration on the morphology of spray-coated TiO$_2$, with the Methanol-Enhanced TiO$_2$ catalyst demonstrating improved structural stability and a more effective photocatalytic surface. Additionally, the TiO$_2$ NTA sample, developed via electrophoretic deposition, presents a structurally superior alternative, offering a compact, uniform layer that maximizes active site exposure and enhances photocatalytic efficiency.

3.1.2. Crystallographic Composition. XRD analysis of Methanol-Enhanced TiO$_2$, Bare-Coated TiO$_2$ and TiO$_2$ NTA confirms the presence of crystalline anatase identification peaks of the TiO$_2$ phases, with variations in peak intensity and broadening indicative of structural differences. The diffraction patterns were used for phase identification, while crystallite sizes were estimated using the Scherrer equation.

The diffraction peaks for TiO$_2$ NTA, Methanol-Enhanced TiO$_2$ and Bare-Coated TiO$_2$ appear in Figure 3 at 2θ values of
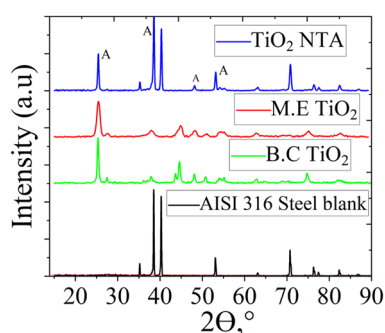
Figure 3. XRD pattern of various TiO$_2$-coated catalysts.

25.42, 37.9, 48.0, 53.9, and 62.6°,[49,50] corresponding to the anatase TiO$_2$ (101), (004), (200), (105), and (204) planes, respectively, as identified using the PDF-4 database, ICDD Card No 03−065−3362 (International Center for Diffraction Data, ICDD).[51] The presence of these peaks confirms that all coatings retain a predominantly anatase structure, which is essential for photocatalytic applications because of their high charge-separation efficiency and stability under UV irradiation. Anatase exhibits superior photocatalytic activity compared to

rutile. Its enhanced crystallinity reduces defect sites that facilitate electron−hole recombination.[52]

The crystallite sizes were estimated using the Scherrer eq (eq 2), which considers peak broadening. The calculated values shown in Figure 4 indicate that Methanol-Enhanced
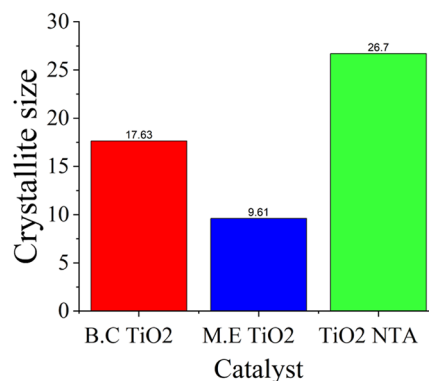
Figure 4. Calculated crystallite sizes of the various TiO$_2$-coated samples.

TiO$_2$ has the smallest crystallite size of 9.61 nm, which suggests a higher surface area and potentially enhanced photocatalytic activity. The Bare-Coated TiO$_2$ sample has an intermediate crystallite size of 17.63 nm, balancing crystallinity and reactivity. In contrast, TiO$_2$ NTA exhibits the largest crystallite size at 26.70 nm, implying a more ordered crystalline structure that may facilitate charge transport but reduce the active surface area available for photocatalysis.

These findings suggest that the different TiO$_2$ coatings exhibit varying degrees of crystallinity and structural properties, which could influence their photocatalytic performance. The smaller crystallite size in Methanol-Enhanced TiO$_2$ may enhance its reactivity due to the increased surface area, while the larger crystallite size in TiO$_2$ NTA may contribute to stability and efficient charge carrier transport. The differences in crystallographic properties highlight the importance of optimizing coating parameters to achieve an ideal balance between surface area, crystallinity, and photocatalytic efficiency.[35]

3.1.3. Effect of Methanol Volume on TiO$_2$ Concentration. The relationship between methanol volume and TiO$_2$ concentration followed a nonlinear trend, indicating dynamic dispersion and aggregation effects. The variations in TiO$_2$ concentration at different methanol levels, including stability, peak dispersion, aggregation, and partial redispersion, are detailed in Table 3. At 0.5 and 1.0 mL, TiO$_2$ concentration remained stable at 0.0116 mol/L, suggesting minimal impact on dispersion. At 1.5 mL, TiO$_2$ concentration peaked at 0.0204 mol/L, indicating optimal dispersion and stabilization,

Table 3. Effect of Methanol Concentration on TiO$_2$ Dispersion and Stability

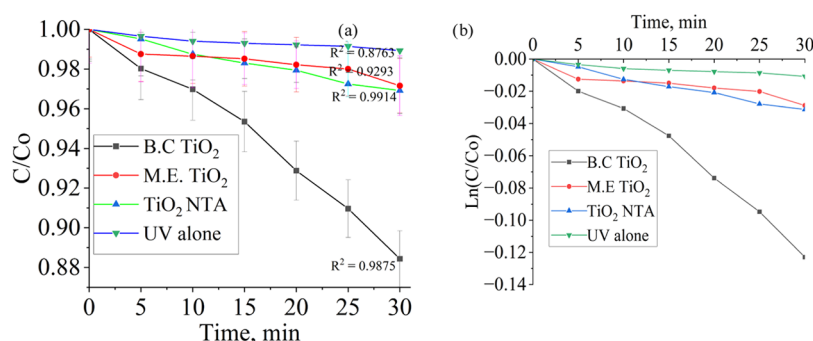| methanol concentration (mL)	TiO$_2$ dispersion (mol/L)
0.5	0.0116
1.0	0.0116
1.5	0.0204
3.0	0.0079
4.5	0.0168
6.0	0.0104

Figure 5. (a) Methylene blue degradation and (b) pseudo-first-order reaction kinetics versus time.
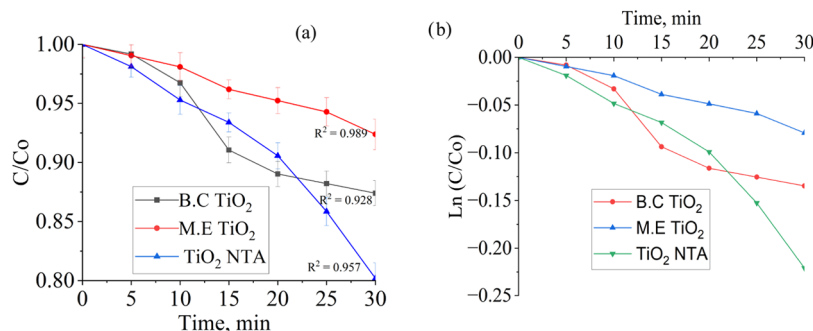

Figure 6. (a) CIP adsorption and (b) pseudo-first-order reaction kinetics versus time.

enhancing surface coverage on AISI 316 steel. However, at 3.0 mL, a sharp decline to 0.0079 mol/L suggested excessive methanol caused aggregation and sedimentation. A partial recovery at 4.5 mL (0.0168 mol/L) implied limited redispersion, while at 6.0 mL (0.0104 mol/L), the system stabilized, showing no further dispersion improvement. These findings highlight methanol's critical yet nonlinear role in TiO_2 dispersion, with 1.5 mL as the optimal volume for achieving uniform coatings and maximizing photocatalytic performance.

3.2. Photocatalytic Performance of TiO_2 Coatings.
3.2.1. Methylene Blue Degradation. In this study, the degradation of MB under UV irradiation was investigated using three TiO_2-coated samples (Bare-Coated TiO_2, Methanol-Enhanced TiO_2, and TiO_2 NTA) alongside a control using UV alone. The samples were assessed for their photocatalytic activity based on initial and final MB concentrations after a 30 min irradiation period.

For the Bare-Coated TiO_2 sample, which contained 2.5 g of TiO_2 and no added methanol in the coating solution, Figure 5a shows the initial MB concentration was 9.754 ± 0.016 mg mg/L, decreasing to 8.626 ± 0.012 mg/L after 30 min under UV irradiation. This translates to a degradation efficiency of approximately 11.57%, indicating a substantial photocatalytic effect compared to photocatalysis alone. The corresponding SEM image shows a cracked surface morphology, suggesting possible issues with structural stability, which may influence the longevity of the coating in repeated use. Despite this, the Bare-Coated TiO_2 sample exhibited the steepest decline in MB concentration, marking it as the most effective among the spray-coated samples in terms of immediate degradation.[53]

The Methanol-Enhanced TiO_2 sample, starting at an MB concentration of 9.503 ± 0.014 mg/L and decreasing to 9.233 ± 0.013 mg/L, achieved a degradation efficiency of 2.84%. This performance is slightly lower than that of the TiO_2 NTA, which degraded MB by approximately 3.08% (from $9.549 \pm$

0.015 to 9.255 ± 0.014 mg/L). The SEM analysis of the Methanol-Enhanced TiO_2 sample revealed a more uniform surface morphology compared to the Bare-Coated sample, likely contributing to its stability during photocatalytic testing. Although its degradation efficiency was lower than the Bare-Coated TiO_2 sample, the Methanol-Enhanced TiO_2 sample remained comparable to values reported in similar studies (6.18% in 30 min),[54] (75.43% mineralization after 90 min)[55] comparable to the well-established TiO_2 NTA.[53]

The slightly lower efficiency may be attributed to the role of methanol in the coating process. While methanol promotes smoother and more stable films, it may also reduce surface defects or active sites that are critical for photocatalysis.[56] On the contrary, the Bare-Coated TiO_2 sample, despite its cracked surface, likely offers greater surface area and reactivity. This highlights the trade-off between immediate degradation efficiency and long-term coating durability.

The TiO_2 NTA sample, which serves as a benchmark due to its proven photocatalytic efficiency,[35,57] exhibited a slight advantage over the Methanol-Enhanced TiO_2 sample, with a total degradation of 3.08%. This marginal difference suggests that the spray-coated Methanol-Enhanced TiO_2 sample, though simpler in application, approaches the effectiveness of the TiO_2 NTA in terms of MB degradation. The high R^2 values in Figure 5a and consistent decline in concentration over time further confirm the TiO_2 NTA's reliability and photocatalytic stability.[57]

The UV-alone control showed a minimal decrease in MB concentration, from 9.589 ± 0.017 to 9.486 ± 0.015 mg/L, resulting in a degradation efficiency of just 1.07%. This low rate of degradation highlights the limited effect of UV irradiation without a photocatalyst, as demonstrated by the nearly flat trend line.[57]

In summary, while the Bare-Coated TiO_2 sample exhibited the highest MB degradation rate, its cracked morphology raises
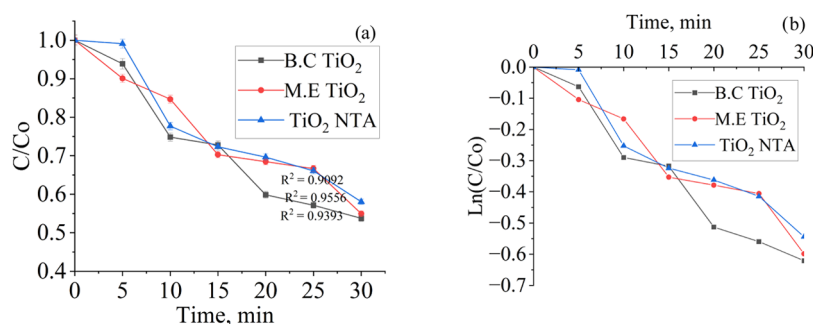
Figure 7. (a) CIP photocatalysis and (b) pseudo-first-order reaction kinetics versus time.

concerns regarding durability under prolonged use. The Methanol-Enhanced TiO$_2$ sample demonstrated a degradation performance comparable to that of the TiO$_2$ NTA, suggesting that spray-coating TiO$_2$ with methanol may serve as a viable alternative to electrophoretic deposition. The findings indicate that optimizing methanol content in spray-coated TiO$_2$ could balance degradation efficiency and coating stability, presenting a promising avenue for scalable photocatalytic applications.

3.2.2. Adsorption on Catalyst. The adsorption of ciprofloxacin (CIP) on various TiO$_2$-coated samples was analyzed to evaluate how their preparation methods influence their ability to remove CIP from the solution. This section focuses on the comparative performance of Bare-Coated TiO$_2$, Methanol-Enhanced TiO$_2$, and TiO$_2$ NTA samples during a 30 min adsorption experiment. By examining the initial and final CIP concentrations, alongside adsorption efficiencies and R^2 values, insights into the relationship between coating morphology and adsorption behavior can be drawn. The aim is to identify the factors contributing to the observed differences and to determine which coating method provides the most effective surface for CIP adsorption.

In Figure 6a, ciprofloxacin (CIP) adsorption on three TiO$_2$-coated samples (Bare-Coated TiO$_2$, Methanol-Enhanced TiO$_2$, and TiO$_2$ NTA) was investigated over 30 min. The initial and final CIP concentrations were recorded to assess the adsorption efficiency for each sample.

For the Bare-Coated TiO$_2$ sample, the CIP concentration started at 0.952 ± 0.012 mg/L and decreased to 0.832 ± 0.015 mg/L, indicating an adsorption efficiency of approximately 12.6%. The R^2 value of 0.928 suggests a moderate linear fit, reflecting some variability in adsorption behavior.

The Methanol-Enhanced TiO$_2$ sample had an initial CIP concentration of 1.049 ± 0.011 mg/L, which decreased to 0.969 ± 0.013 mg/L, resulting in an adsorption efficiency of around 7.6%. This is the lowest adsorption efficiency observed among the samples, indicating a reduced adsorption affinity for CIP. However, the R^2 value of 0.989 reflects a strong linear fit, suggesting a consistent adsorption pattern throughout the experiment.[53]

The TiO$_2$ NTA sample showed a CIP concentration reduction from 1.059 ± 0.012 to 0.849 ± 0.014 mg/L, yielding an adsorption efficiency of approximately 19.8%. This sample achieved the highest adsorption efficiency among the three, with an R^2 value of 0.957, indicating a reliable and consistent adsorption performance.[35]

In summary, the TiO$_2$ NTA sample demonstrated the highest adsorption efficiency for CIP, followed by the Bare-Coated TiO$_2$ sample, with the Methanol-Enhanced TiO$_2$ sample showing the lowest efficiency. This trend suggests

that the specific preparation methods impact the surface characteristics of TiO$_2$, thereby influencing CIP adsorption. The results underscore the superior adsorption capacity of the TiO$_2$ NTA in comparison to the spray-coated samples.

3.2.3. Photocatalytic Degradation Study. Figure 7 illustrates the model wastewater degradation of 1 mg/L ciprofloxacin (CIP) over time with photocatalysis under three different experimental conditions: Bare-Coated TiO$_2$, Methanol-Enhanced TiO$_2$, and TiO$_2$ NTA samples. The degradation process for each condition is represented by a linear regression fit, with the corresponding R^2 values provided to indicate the strength of the correlation between time and CIP concentration. This analysis highlights the differences in catalytic performance and degradation pathways, offering insights into the role of coating preparation and catalyst activity in wastewater treatment applications.

The degradation efficiency can be analyzed based on the observed decrease in CIP concentration over time. For TiO$_2$ NTA, the final concentration after 30 min is higher (~0.66 ± 0.012 mg/L), suggesting lower degradation compared to the other setups. The Methanol-Enhanced TiO$_2$ catalyst demonstrates the steepest decline in CIP concentration, highlighting its enhanced wastewater degradation performance due to the catalyst's activity. Meanwhile, the Bare-Coated TiO$_2$ catalyst, while still showing some degradation, exhibits a slower rate and a less steep slope compared to the Methanol-Enhanced TiO$_2$ catalyst. This comparison underscores the significant role of the catalyst in accelerating and improving the degradation process.

The R^2 values not only reflect the linearity of the degradation process but also provide insight into the reliability of the reaction kinetics. A higher R^2, as seen with the Methanol-Enhanced TiO$_2$ catalyst, indicates a more controlled and uniform degradation pathway. The lower R^2 for the TiO$_2$ NTA and Bare-Coated TiO$_2$ catalyst suggests less consistent reaction kinetics, possibly due to variations in the reaction conditions or limited availability of catalytic surfaces. Overall, the presence of the catalyst enhances both the degradation efficiency and the consistency of the reaction,[57] making the Methanol-Enhanced TiO$_2$ catalyst the most effective condition for CIP degradation in this experiment.

The superior performance of M.E TiO$_2$ coating in both CIP adsorption (7.6%) and photocatalytic degradation can be attributed to the interaction between modified surface chemistry and CIP's molecular structure. Methanol acts as a structure-directing agent, promoting the formation of a more uniform and hydroxyl-rich TiO$_2$ surface, which improves the availability and surface polarity of the active site.[58] This favors the adsorption of polar molecules containing heteroatoms such
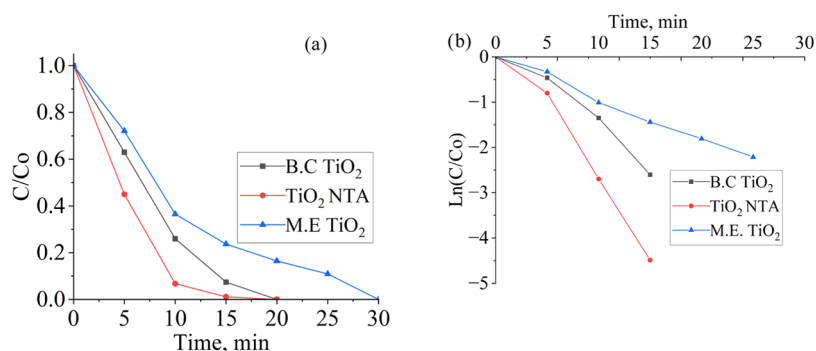
Figure 8. (a) Photocatalytic ozonation of CIP wastewater and (b) pseudo-first-order reaction kinetics versus time.
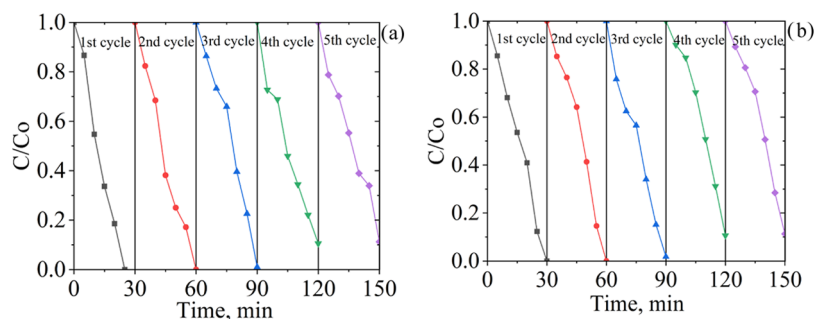
Figure 9. Photocatalytic degradation of CIP during cyclic reuse of photocatalyst (a) TiO_2 NTA and (b) Methanol-Enhanced TiO_2.

as CIP through hydrogen bonding and $\pi-\pi$ interactions.[59,60] Additionally, CIP's complex structure with electron-donating groups facilitates stronger charge transfer interactions, which, combined with reduced electron–hole recombination on the methanol-modified surface, leads to a higher generation of reactive oxygen species (ROS).[61] These synergistic effects explain the steep decrease in CIP concentration and suggest that Methanol-Enhanced TiO_2 selectively favors the degradation of structurally complex pharmaceutical pollutants over-simpler dyes such as MB.

This section explores the accelerated degradation of 1 mg/L ciprofloxacin (CIP) under UV and ozone (photocatalytic ozonation) for three TiO_2-coated samples: Bare-Coated TiO_2, Methanol-Enhanced TiO_2, and TiO_2 NTA. The study examines the combined effects of UV and ozone in driving CIP degradation, focusing on the enhanced reaction dynamics, reduced degradation times, and the ability to achieve complete removal of CIP. This analysis compares the performance of each catalyst in this advanced oxidation setup to prior results without ozone in Figure 7, offering insights into the synergistic role of UV and ozone in wastewater treatment applications.[62]

In Figure 8, the degradation of 1 mg/L CIP under UV and Ozone is significantly accelerated for all conditions compared to the previous experiment without ozone as shown in Figure 7. The Bare-Coated TiO_2 catalyst and the TiO_2 NTA conditions achieve complete degradation within 20 min, demonstrating the powerful oxidative effects of UV and ozone even in the absence of or with minimal catalyst involvement.[63] For the Methanol-Enhanced TiO_2 catalyst condition, complete wastewater degradation occurs within 30 min, indicating a slightly slower but still highly effective degradation process.

The observed performance contrasts with the first experiment in Figure 7, where neither the Bare-Coated TiO_2 catalyst nor the TiO_2 NTA catalyst conditions achieved complete

degradation, regardless of the time. In that earlier scenario, the Methanol-Enhanced TiO_2 catalyst condition showed the most effective degradation but still did not reach complete removal of CIP within the 30 min time frame. The addition of Ozone in this experiment not only boosts the wastewater degradation rates for all conditions but also ensures that complete degradation is achieved for every condition, albeit at slightly different times.[57]

The differences in degradation timing highlight how the introduction of ozone shifts the dynamics of the reaction.[57] For the Bare-Coated TiO_2 catalyst and the TiO_2 NTA conditions, these oxidative processes compensate for the absence or lower concentration of a catalyst, driving rapid and complete CIP removal. In the case of the Methanol-Enhanced TiO_2 catalyst condition, the degradation trend remains strong and consistent, but the additional oxidative effects of UV and ozone appear to moderate the relative impact of the catalyst,[62] resulting in complete degradation occurring slightly later than in the other two setups.

The synergistic enhancement via $^\bullet$OH radical generation of OH radicals during ozonation is supported by both the literature and our previous work. Ozone interacts with the surfaces of the water and the catalyst to produce hydroxyl radicals,[64] which are highly reactive species responsible for the rapid degradation of pollutants.[65] Our previously published study[57] experimentally confirmed significant $^\bullet$OH radical generation of OH radicals during ozonation, validated by scavenger tests, thus underpinning the proposed mechanism of ozone–TiO_2 synergy through hydroxyl radical-mediated oxidation. Recent findings further reinforce this mechanism: direct photolysis of ozone under UV light forms excited-state $O(^1D)$, which reacts with water to yield $^\bullet$OH radicals,[66] while modified TiO_2 surfaces enhance ozone activation and ROS production via electron-mediated pathways.[67,68]
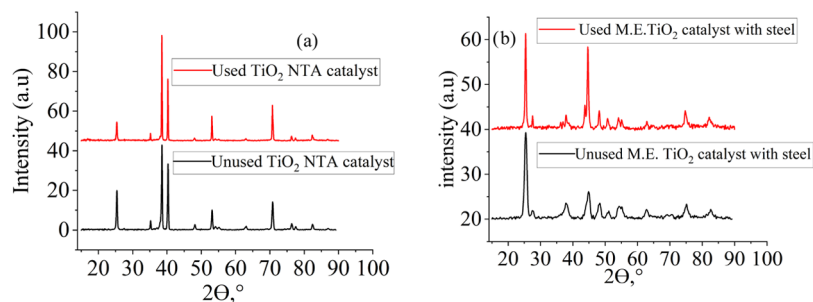
Figure 10. XRD analysis (a) TiO_2 NTA catalysts and (b) Methanol-Enhanced TiO_2 catalysts.
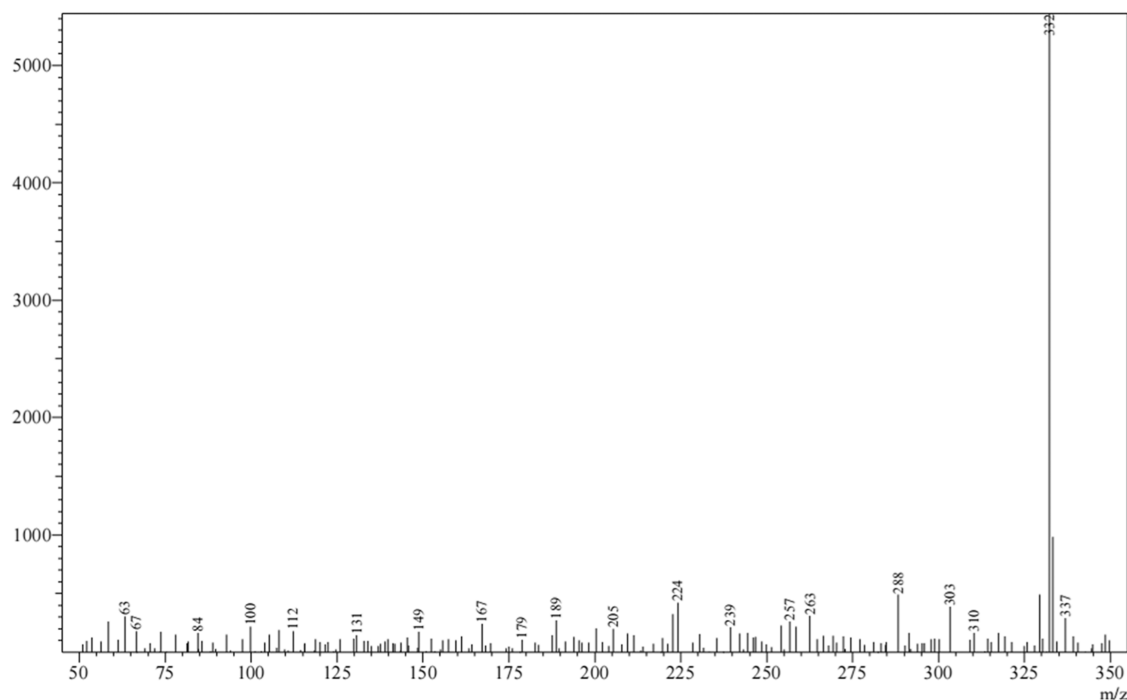

Figure 11. Mass spectrum of sample containing CIP at time $t = 0$.

Overall, when comparing both experiments, the incorporation of UV and ozone dramatically enhances the efficiency of CIP degradation, enabling complete removal in all conditions, which was unattainable without these advanced oxidation processes. This emphasizes the critical role of UV and ozone in accelerating degradation, particularly in conditions where the catalytic effect alone is insufficient.[57]

In summary, the addition of UV and ozone led to a 33.33% reduction in the time required for complete degradation under the Bare-Coated TiO_2 catalyst and the TiO_2 NTA conditions, demonstrating the powerful oxidative effect of these advanced processes. The slight delay in the Methanol-Enhanced TiO_2 catalyst condition reaching complete degradation suggests potential interactions between the catalyst and oxidative processes that merit further investigation.

3.2.4. Reusability and Stability Testing. Figure 9 evaluates the reusability and degradation efficiency of ciprofloxacin (CIP) in wastewater treatment using Methanol-Enhanced TiO_2 and TiO_2 NTA samples across five consecutive cycles, each lasting 30 min. The Bare-Coated TiO_2 sample was not tested for reusability because the study focused on evaluating the performance of Methanol-Enhanced TiO_2 as a potential alternative to TiO_2 NTA, with the primary emphasis on photocatalytic effectiveness and durability rather than the

reusability of Bare-Coated TiO_2. The study aims to determine how well the catalytic performance of each system is maintained over repeated use, emphasizing long-term reusability and scalability. By analyzing reusability, this section highlights the robustness and degradation efficiency of these photocatalytic systems under cyclic operational conditions.

For the TiO_2 NTA sample (Figure 9a), the first and second cycles achieved 100% degradation. By the fifth cycle, the initial concentration of 1.088 mg/L was reduced to 0.122 mg/L, achieving an 88.75% degradation efficiency. Comparing the first and fifth cycles, the efficiency difference was 11.25%. Between the fourth and fifth cycles, where the initial concentrations were 1.137 and 1.088 mg/L, respectively, the efficiency difference was only 0.7%, indicating good reusability.[57,69]

For the Methanol-Enhanced TiO_2 (Figure 9b), the first and second cycles achieved 100% degradation. By the fifth cycle, the initial concentration of 1.080 mg/L was reduced to 0.122 mg/L, achieving 88.72% degradation efficiency. Comparing the first and fifth cycles, the efficiency difference was 11.28%. Between the fourth and fifth cycles, where the initial concentrations were 1.1272 and 1.080 mg/L, respectively, the efficiency difference was 0.68%, again demonstrating good reusability.
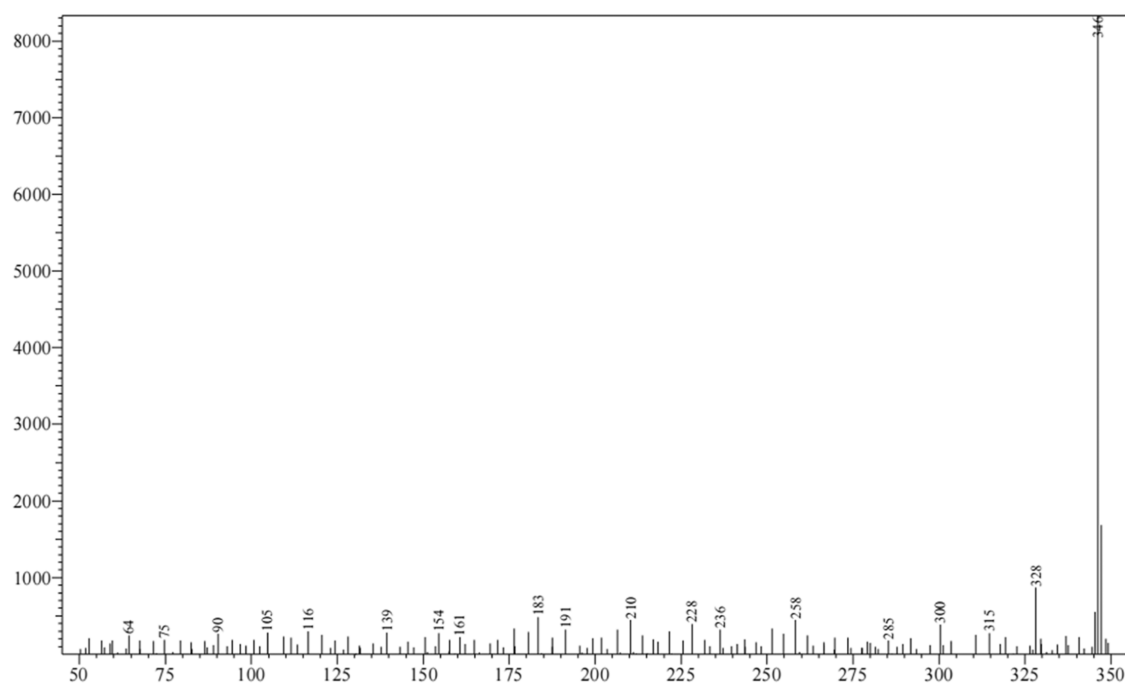
Figure 12. Mass spectrum of sample containing degraded CIP with TiO$_2$ NTA.

These findings reveal that both the TiO$_2$ NTA sample and Methanol-Enhanced TiO$_2$ catalyst maintain high degradation efficiencies across multiple cycles,[69,70] with the TiO$_2$ NTA sample slightly outperforming the sprayed alternative in long-term reusability. Nonetheless, the minimal efficiency differences between the fourth and fifth cycles for both catalysts confirm their potential for scalability in repeated applications.[57]

The structural stability of the catalysts was further examined by XRD analysis (Figure 10). The characteristic diffraction peaks for both catalysts remained practically unchanged after multiple cycles, confirming the preservation of the crystallite phase composition. However, there is a slight broadening of the peaks in the unused M.E. TiO$_2$ sample suggesting a minor structural disorder or incomplete crystallization in the prepared state. Interestingly, with the used M.E. TiO$_2$, the peaks became sharper and more intense, indicating a possible recrystallization or ordering effect during prolonged UV exposure.[71,72] This behavior could result from the removal of residual organics derived from methanol, photothermal annealing, or relaxation of microstrain within the TiO$_2$ lattice, which collectively enhance crystallinity. In contrast, TiO$_2$ NTA exhibited a more stable crystalline structure with repeated use.

Overall, these findings demonstrate good reusability potential for both catalysts. Although TiO$_2$ NTA remains the stronger candidate in terms of long-term phase stability, the Methanol-Enhanced TiO$_2$ catalyst exhibited comparable photocatalytic efficiency, indicating favorable prospects for scalable wastewater treatment applications.

3.2.5. Analytical Identification of Intermediate Products. The photocatalytic degradation of ciprofloxacin (CIP) was analyzed using two experimental systems: Methanol-Enhanced TiO$_2$, and TiO$_2$ NTA samples. HPLC-MS analysis provided critical insights into the degradation pathways and byproduct formation in these setups.

The MS spectrum at 0 min (Figure 11) shows a dominant base peak at 332 (+) m/z, corresponding to the intact molecular ion of ciprofloxacin. This confirms the initial presence and purity of ciprofloxacin in solution before any photocatalytic treatment. The presence of this peak as the base ion (highest intensity) indicates no prior degradation or transformation at the beginning of the experiment. Additional fragments at 288 (+) m/z,[61] 263 (+) m/z,[61] and 224 (+) m/z suggest early stage fragmentation patterns but indicate no significant degradation of the parent compound. These are typical early stage fragments of ciprofloxacin and are consistent with loss of water, carboxyl groups, or cleavage of the piperazine ring. The presence of a well-defined peak at 332 (+) m/z confirms the initial concentration before photocatalytic treatment.

Following exposure to photocatalysis using TiO$_2$ NTA (Figure 12), the base peak at 346 (+) m/z[35,73] dominates, indicating oxidative defluorination and hydroxylation. The disappearance of 332 (+) m/z suggests rapid degradation of CIP under photocatalytic conditions. This shift demonstrates that TiO$_2$ NTA effectively promotes CIP breakdown, initiating oxidative defluorination, and leading to the formation of multiple degradation products. Fragment ions at 328 (+) m/z, 315 (+) m/z, and 285 (+) m/z, indicate key degradation processes, including oxidative defluorination, piperazine ring cleavage, and decarboxylation. Specifically, 328 (+) m/z and 315 (+) m/z suggest sequential defluorination and fragmentation of the CIP molecule,[74] while 285 (+) m/z corresponds to the breakdown of the piperazine ring and loss of functional groups such as ethyl or carboxylic groups.[75,76] In addition to these key peaks, the spectrum shows a wide range of lower-intensity fragments below m/z 200, such as peaks at 64, 75, 105, 139, 154, 183, and others. These low m/z values reflect extensive breakdown of the molecular structure, indicating a progressive mineralization of organic intermediates into smaller and less complex species. The broad distribution of lower m/z fragments implies extensive mineralization of the CIP, strengthening TiO$_2$ NTA's strong photocatalytic activity. The results of mass spectrometry confirm that TiO$_2$ NTA facilitates an efficient degradation pathway for CIP, involving:
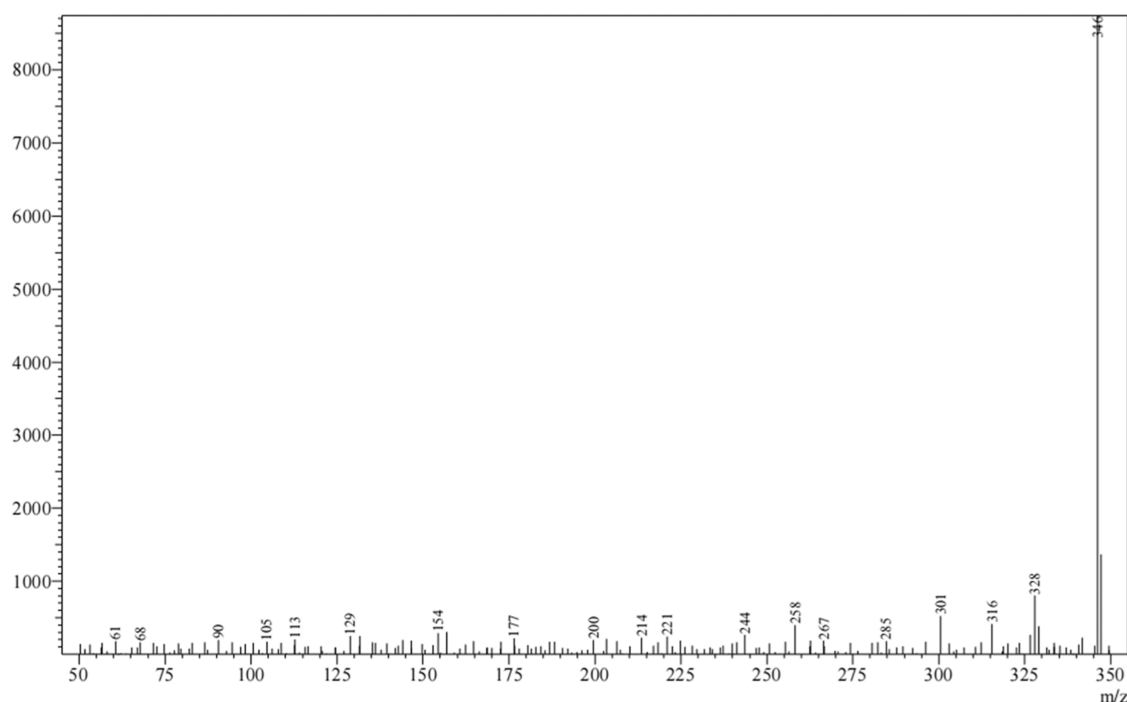
Figure 13. Mass spectrum of sample containing degraded CIP with Methanol-Enhanced TiO_2.

Oxidative defluorination, cleavage of the piperazine ring, decarboxylation, hydrolation, progressive fragmentation, and mineralization.

The MS spectrum for Methanol-Enhanced TiO_2 (Figure 13) also revealed the disappearance of 332 (+) m/z but with a distinct degradation pattern. The base peak remains at 346 (+) m/z,[61] indicating the formation of a stable hydroxylated or defluorinated transformation product, although with less extensive fragmentation overall. Peaks at 328 (+) m/z, 316 (+) m/z[52] and 301 (+) m/z[77] suggest the presence of early stage oxidation intermediates, such as monodefluorinated species or partially cleaved side chains. Unlike TiO_2 NTA, the spectrum lacks strong signals in the lower m/z range, with only minor peaks at 285, 238, 177, and 154 m/z, reflecting a limited degree of molecular breakdown. This pattern implies that degradation is proceeding at a slower rate, with incomplete mineralization of the parent compound. The reduced intensity of low-mass fragments suggests that methanol modification may inhibit deeper oxidative cleavage, potentially by scavenging reactive oxygen species (ROS), such as hydroxyl radicals. This alteration in degradation behavior indicates that methanol-modified TiO_2 influences photocatalytic pathways, likely affecting ROS generation and reactivity, and thus modulating overall degradation kinetics.[78,79] The proposed degradation intermediates and their corresponding mass-to-charge ratios (m/z) are summarized in Table 4 below.

3.2.5.1. Comparison of Degradation Pathways. The comparative results between TiO_2 NTA and Methanol-Enhanced TiO_2 reveal distinct differences in their photocatalytic efficiencies. TiO_2 NTA exhibits a higher degree of fragmentation, with a more pronounced breakdown of ciprofloxacin into lower m/z intermediates. The presence of multiple low-mass peaks suggests an aggressive oxidative environment that facilitates rapid decomposition of the antibiotic. This indicates that TiO_2 NTA generates a more

reactive surface, leading to faster mineralization of the parent compound. The strong photocatalytic activity of TiO_2 NTA can be attributed to its ordered nanotubular structure, which enhances charge separation and prolongs electron−hole pair lifetimes, leading to more efficient ROS generation.

On the other hand, Methanol-Enhanced TiO_2 shows a more controlled degradation process, with fewer detected intermediates and a less intense fragmentation pattern. The retention of certain high m/z species suggests a different degradation mechanism, possibly favoring selective oxidation rather than complete mineralization. The presence of methanol in the coating process may have altered the electronic properties of the TiO_2 surface, affecting charge carrier dynamics and ROS production. This could explain why Methanol-Enhanced TiO_2 degrades ciprofloxacin at a slower rate compared to TiO_2 NTA. However, its ability to produce transformation products at a measured pace may be advantageous in applications where controlled degradation is preferred to prevent the formation of harmful byproducts.

Additionally, the methanol modification may have influenced the hydrophilicity of the TiO_2 coating, affecting its interaction with water and contaminants. This could lead to differences in adsorption dynamics, which in turn impact the efficiency of photocatalytic degradation. While TiO_2 NTA aggressively breaks down ciprofloxacin into multiple byproducts, Methanol-Enhanced TiO_2 might allow for a more gradual degradation pathway, potentially reducing the risk of sudden accumulation of toxic intermediates in treated water.

4. CONCLUSIONS

The findings of this study highlight the importance of optimized TiO_2 coatings on AISI 316 steel in enhancing photocatalytic wastewater treatment. The TiO_2 NTA coatings demonstrated superior structural integrity, achieving an 88.75% degradation efficiency for ciprofloxacin (CIP) by the fifth reuse cycle, with only an 11.25% reduction in performance

Table 4. Major Byproducts Detected by LC-MS during Photocatalytic Degradation of Ciprofloxacin
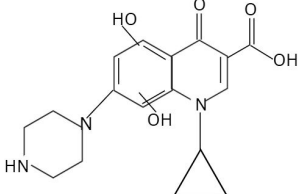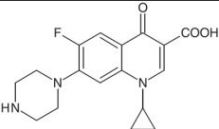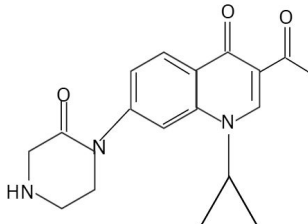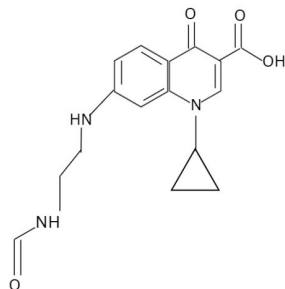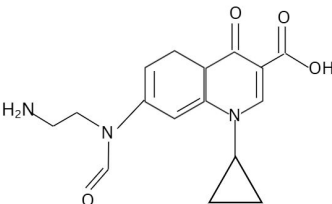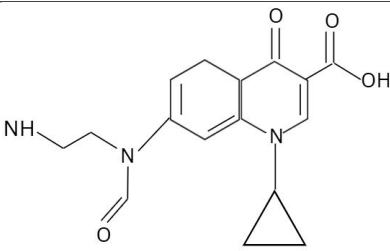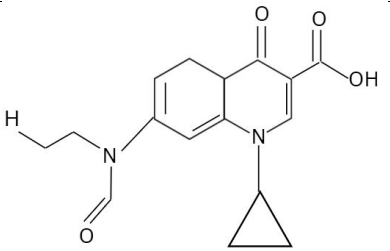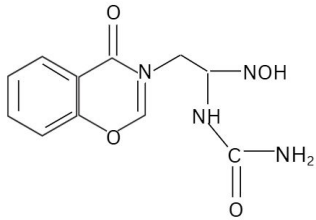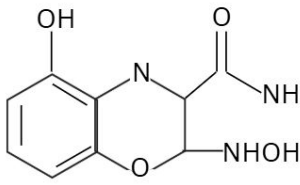
By product ciprofloxacin	Observed peak (m/z)	Degradation pathway	References
x,y-dihydroxy-1-cyclopropyl-6-fluoro-4-oxo-7-piperazin-1-ylquinoline-3-carboxylic acid	346	Oxidative defluorination and hydroxylation	Abromaitis et al, 2022 [35] Kovačević et al, 2024 [61] Tang et al 2024 [73]
Ciprofloxacin	332	-	-
1-cyclopropyl-6,7-dioxo-1,4-dihydroquinoline-3-carboxylic acid, piperazin-1-yl amide derivative	328	Oxidative defluorination, Ring hydroxylation and oxidation	Nair et al, 2024 [74]
1-cyclopropyl-7-[(2-formamidoethyl)amino]-4-oxo- 1,4-dihydroquinoline-3-carboxylic acid Or 7-[N-(2-aminoethyl)formamido]-1-cyclopropyl-4-oxo-1,4-dihydroquinoline-3-carboxylic acid	316	Defluorination, piperazine cleavage and decarboxylation	Odling and Robertson, 2015 [52]

Table 4. continued

By product ciprofloxacin	Observed peak (m/z)	Degradation pathway	References
1-Cyclopropyl-6-fluoro-7-(2-aminoethylamido)-4-oxoquinoline-3-carboxylic acid	315	cleavage of the piperazine ring, amide formation	Nair et al, 2024 [74]
1-Cyclopropyl-6-fluoro-7-formamido-4-oxoquinoline-3-carboxylic acid	301	dealkylation or oxidative cleavage	Usman et al, 2021 [77]
N-Hydroxyethyl-quinoline-3-carboxamide **Or** 2-Hydroxy-1,4-dihydroquinoline-3-carboxamide, N'-hydroxy-N-methylhydrazide derivative	285	defluorination, piperazine ring cleavage, and partial oxidation	Noroozi et al, 2023 [75] Liu et al, 2024, [76]

from the first cycle. Methanol-Enhanced TiO$_2$ coatings, although slightly less structurally cohesive, exhibited advanced photocatalytic activity, with degradation efficiency remaining high at 88.72% by the fifth cycle. In contrast, Bare-Coated TiO$_2$, characterized by a cracked and uneven morphology, displayed significantly lower adsorption and degradation performance, underscoring the importance of optimized coating techniques.

Under UV light, Methanol-Enhanced TiO$_2$ achieved rapid CIP degradation, including near-complete mineralization within 10 min, facilitated by secondary radical-driven reactions. When Ozone was introduced, all coating systems achieved complete CIP degradation. For the Bare-Coated TiO$_2$ and TiO$_2$ NTA systems, degradation was completed within 20 min, while the Methanol-Enhanced TiO$_2$ system required 30 min, reflecting a slight interaction between the catalyst and ozone-enhanced processes.

The HPLC-MS analysis revealed distinct degradation mechanisms: TiO$_2$ NTA facilitated rapid fragmentation of CIP, producing multiple low m/z intermediates that indicated

aggressive oxidative breakdown. Methanol-Enhanced TiO_2, in contrast, exhibited a more controlled degradation pathway with key transformation peaks at 316 (+) m/z and 285 (+) m/z, suggesting selective oxidation and progressive mineralization rather than immediate fragmentation. This approach may reduce the risk of accumulating toxic byproducts, making it a promising strategy for sustainable pollutant removal.

Overall, the TiO_2 NTA coatings set a benchmark for structural stability and reuse potential, while Methanol-Enhanced TiO_2 coatings demonstrated exceptional catalytic activity and a refined degradation process. These results establish a framework for tailoring TiO_2 coatings to meet industrial-scale wastewater treatment needs, offering a balance between efficiency, durability, and scalability.

■ AUTHOR INFORMATION

Corresponding Author

  Maria-Anthoniette Oghenetejiro Onoriode-Afunezie — *Kaunas University of Technology, Kaunas, Faculty of Chemical Technology, LT-50254 Kaunas, Lithuania;* ⊙ orcid.org/0000-0002-4220-4250; Email: maria.onoriode@ktu.edu

Authors

  Povilas Urbanskis — *Kaunas University of Technology, Kaunas, Faculty of Chemical Technology, LT-50254 Kaunas, Lithuania*

  Inga Urniežaitė — *Kaunas University of Technology, Faculty of Chemical Technology, LT-50254 Kaunas, Lithuania*

  Agnė Šulčiūtė — *Kaunas University of Technology, Kaunas, Faculty of Chemical Technology, LT-50254 Kaunas, Lithuania;* ⊙ orcid.org/0000-0002-2771-5845

Complete contact information is available at:
https://pubs.acs.org/10.1021/acsomega.5c03565

Notes

The authors declare no competing financial interest.

■ REFERENCES

(1) Dhull, P.; Saini, N.; Aamir, M.; Parveen, S.; Husain, S. Function of Nanomaterials in the Treatment of Emerging Pollutants in Wastewater. In *Detection and Treatment of Emerging Contaminants in Wastewater*; IWA Publishing, 2024.

(2) Rana, K.; Kaur, H.; Singh, N.; Sithole, T.; Siwal, S. S. Graphene-Based Materials: Unravelling Its Impact in Wastewater Treatment for Sustainable Environments. *Next Mater.* **2024**, *3*, No. 100107.

(3) Bi, J.; Dong, G. Wastewater Treatment: Functional Materials and Advanced Technology. *Molecules* **2024**, *29* (9), No. 2150.

(4) *Advanced Materials for Emerging Water Pollutant Removal*; Pei, S. G.; Devagi, K.; Anwar, I.; Ahmad, F. I., Eds.; Royal Society of Chemistry, 2024; Vol. 14.

(5) Inamdar, A. K.; Inamdar, S. A.; Birajdar, C. T.; Bhale, J.; Rajmane, S. V.; Shinde, B. H.; Patole, S. P.; Shelke, S. B.; Inamdar, S. N. Applications of Titanium Dioxide (TiO2) Nanoparticles in Photocatalysis. *Sci. Adv. Mater.* **2024**, *16* (7), 757−771.

(6) Gatou, M.-A.; Syrrakou, A.; Lagopati, N.; Pavlatou, E. A. Photocatalytic TiO2-Based Nanostructures as a Promising Material for Diverse Environmental Applications: A Review. *Reactions* **2024**, *5* (1), 135−194.

(7) Kong, E. D. H.; Chau, J. H. F.; Lai, C. W.; Khe, C. S.; Sharma, G.; Kumar, A.; Siengchin, S.; Sanjay, M. R. GO/TiO2-Related Nanocomposites as Photocatalysts for Pollutant Removal in Wastewater Treatment. *Nanomaterials* **2022**, *12* (19), No. 3536.

(8) Göçer, S.; Kozak, M.; Ayranpınar, İ.; Duyar, A.; Köroğlu, E. O.; Cırık, K. Application of titanium dioxide(TiO2) nanoparticle materials on domestic wastewater: removal of pollutants. *Kahramanmaraş Sütçü İmam Üniv. Mühendislik Bilimleri Derg.* **2022**, *25* (4), 570−576.

(9) Sivaraman, C.; Vijayalakshmi, S.; Leonard, E.; Sagadevan, S.; Jambulingam, R. Current Developments in the Effective Removal of Environmental Pollutants through Photocatalytic Degradation Using Nanomaterials. *Catalysts* **2022**, *12* (5), No. 544.

(10) Alam, N.; Uddin, I.; Ihsan, H.; Khan, A.; Ullah, K.; Alam, N.; Uddin, I.; Ihsan, H.; Khan, A.; Ullah, K. A Compendium of Nanomaterials for Corrosion Control: Categorizing Types and Evaluating Their Practical Uses. In *Innovations in Nanomaterials-Based Corrosion Inhibitors*; IGI Global Scientific Publishing, 2024.

(11) El-Sherif, R.; Mahmoud, A. S.; Abd-El-Khalek, D. E.; Khamis, E. Nanomaterials as Next-Gen Corrosion Inhibitors: A Comprehensive Review for Ceramic Wastewater Treatment. *Key Eng. Mater.* **2024**, *983*, 117−124.

(12) Pavel, M.; Anastasescu, C.; State, R.-N.; Vasile, A.; Papa, F.; Balint, I. Photocatalytic Degradation of Organic and Inorganic Pollutants to Harmless End Products: Assessment of Practical Application Potential for Water and Air Cleaning. *Catalysts* **2023**, *13* (2), No. 380.

(13) Sheikhzadeh, M. S.; Ahmadi, R.; Ghamari, N.; Afshar, A. Fabrication of PTFE + TiO2/Ag Coatings on 316L/Polydopamine with Advanced Mechanical, Bio-Corrosion, and Antibacterial Properties for Stainless Steel Catheters. *J. Biomater. Sci., Polym. Ed.* **2024**, *35* (13), 2020−2048.

(14) Ahmed, T.; Farooq, T.; Ahmed, K.; Ur Rehman, M. A.; Yasir, M.; Butt, S.; Basit, M. A. Ensuing the Formation of Photocatalytic TiO2/Fe2O3 Nanocomposite from Heat Treatment of Electrophoretically Deposited TiO2 Films on Stainless Steel. *Colloids Surf., A* **2024**, *691*, No. 133850.

(15) Chaharmahali, R.; Fattah-alhosseini, A.; Karbasi, M.; Giannakis, S.; Bahramian, H.; Oulego, P. A Systematic Study on Modulation of Plasma Electrolytic Oxidation Parameters for Optimizing Photocatalytic Coatings on Titanium Substrates. *J. Alloys Compd.* **2023**, *963*, No. 171234.

(16) Pinton, J. H. B.; Oliveira, A. F.; Huanca, D. R.; Mohallem, N. D. S. Development of an Automated and Cost-Effective Apparatus for Sol-Gel Solution Deposition Using Spray Coating Technique and Its Application for TiO2 Based Photocatalytic Films. *Mater. Chem. Phys.* **2024**, *318*, No. 129213.

(17) Edusi, C.; Sankar, G.; Parkin, I. P. The Effect of Solvent on the Phase of Titanium Dioxide Deposited by Aerosol-Assisted CVD. *Chem. Vap. Deposition* **2012**, *18* (4−6), 126−132.

(18) Wiranwetchayan, O.; Promnopas, S.; Thongtem, T.; Chaipanich, A.; Thongtem, S. Effect of Alcohol Solvents on TiO2 Films Prepared by Sol−Gel Method. *Surf. Coat. Technol.* **2017**, *326*, 310−315.

(19) Thayanithi, S.; Janakiraman, K.; Alagesan, S.; Ramesh, A.; Sethuraman, V.; Prema, S. S. Role of Carbon Nanotubes, Carbon Nano-Fibres and Nano-Gels in Eliminating Pollutants from Aqueous Solution. *Phys. Sci. Rev.* **2024**, *9*, 3347−3368, DOI: 10.1515/psr-2023-0045.

(20) Sushma, C.; Kavitha, R.; Krishna, R. H.; Dsouza, F.; Chandraprabha, M. N.; Kumar, S. G. Plasmonic Photocatalytic Materials for Pollutants Removal. In *Advanced Functional Materials and Methods for Photodegradation of Toxic Pollutants*; Mishra, A. K.;

Singh, P.; Raizada, P.; Vadivel, S.; Selvasembian, R., Eds.; Elsevier, 2024; Chapter 6, pp 129−159.

(21) da Silva Júnior, A. H.; de Oliveira Martins Müller, J.; de Oliveira, C. R. S.; de Noni Junior, A.; Tewo, R. K.; Mhike, W.; da Silva, A.; Mapossa, A. B.; Sundararaj, U. New Insights into Materials for Pesticide and Other Agricultural Pollutant Remediation. *Materials* **2024**, *17* (14), No. 3478.

(22) Kumar, S.; Gupta, T. Utilization of Nanoparticles-Based Corrosion Inhibitor in Various Systems. In *Sustainability, Safety, and Applications of Nanomaterials-Based Corrosion Inhibitors*; IGI Global Scientific Publishing, 2024.

(23) Karabulut, G.; Üllen, N. B.; Karakuş, S. Enhancement of Surface Properties of 316L Stainless Steel with Silver Nanoparticles Using Airbrush Spray Process. *Erzincan Univ. J. Sci. Technol.* **2023**, *16* (2), 357−373.

(24) Cabezuelo, O.; Diego-Lopez, A.; Atienzar, P.; Marin, M. L.; Bosca, F. Optimizing the Use of Light in Supported TiO2 Photocatalysts: Relevance of the Shell Thickness. *J. Photochem. Photobiol., A* **2023**, *444*, No. 114917.

(25) Darvish, S. M.; Masoudi, A. A.; Mortezaali, A.; Hosseini, Z. S. Enhanced Visible Light Photocatalytic Activity of Nanostructured SiO2-TiO2 Thin Films through Optimizing Thickness. *Phys. Scr.* **2023**, *98* (10), No. 105904.

(26) Jose, A.; Yadav, P.; Svirskis, D.; Swift, S.; Gizdavic-Nikolaidis, M. R. Antimicrobial Photocatalytic PANI Based-Composites for Biomedical Applications. *Synth. Met.* **2024**, *303*, No. 117562.

(27) Jadon, M. S.; Kumar, S. Fabrication of TiO2 Nanoparticle Coating on Stainless Steel 316L and Its Assessment for Orthopaedic Applications. *Int. J. Online Biomed. Eng. (iJOE* **2024**, *20* (10), 47−63.

(28) Caselli, L.; Traini, T.; Micciulla, S.; Sebastiani, F.; Köhler, S.; Nielsen, E. M.; Diedrichsen, R. G.; Skoda, M. W. A.; Malmsten, M. Antimicrobial Peptide Coating of TiO2 Nanoparticles for Boosted Antimicrobial Effects. *Adv. Funct. Mater.* **2024**, *34*, No. 2405047, DOI: 10.1002/adfm.202405047.

(29) Di, Y.; Gu, Z.; Kang, Y.; Tian, J.; Hu, C. Enhanced Oxidation of Organic Pollutants by Regulating the Interior Reaction Region of Reactive Electrochemical Membranes. *J. Hazard. Mater.* **2024**, *466*, No. 133584.

(30) Wang, H.; Wang, J.; Bo, G.; Wu, S.; Luo, L. Degradation of Pollutants in Polluted River Water Using Ti/IrO2−Ta2O5 Coating Electrode and Evaluation of Electrode Characteristics. *J. Cleaner Prod.* **2020**, *273*, No. 123019.

(31) Wang, W.-M.; Lu, T.-H.; Chen, C.-Y.; Liao, C.-M. Assessing Microplastics-Antibiotics Coexistence Induced Ciprofloxacin-Resistant *Pseudomonas aeruginosa* at a Water Region Scale. *Water Res.* **2024**, *257*, No. 121721.

(32) Jyoti, K.; Soni, K.; Chandra, R. Pharmaceutical Industrial Wastewater Exhibiting the Co-Occurrence of Biofilm-Forming Genes in the Multidrug-Resistant Bacterial Community Poses a Novel Environmental Threat. *Aquat. Toxicol.* **2024**, *273*, No. 107019.

(33) Yadav, N.; Mandpe, A.; Shukla, S. A Brief Account of the Antibiotics and Antibiotic Resistance Genes in an Aquatic Environment. In *Detection and Treatment of Emerging Contaminants in Wastewater*; IWA Publishing, 2024; Chapter 5.

(34) Dlamini, M. C.; Maubane-Nkadimeng, M. S.; Moma, J. A. The Use of TiO2/Clay Heterostructures in the Photocatalytic Remediation of Water Containing Organic Pollutants: A Review. *J. Environ. Chem. Eng.* **2021**, *9* (6), No. 106546.

(35) Abromaitis, V.; Svaikauskaite, J.; Sulciute, A.; Sinkeviciute, D.; Zmuidzinaviciene, N.; Misevicius, S.; Tichonovas, M.; Urniezaite, I.; Jankunaite, D.; Urbonavicius, M.; Varnagiris, S.; Dzingeleviciene, R.; Baranauskis, K.; Martuzevicius, D. Ozone-Enhanced TiO2 Nanotube Arrays for the Removal of COVID-19 Aided Antibiotic Ciprofloxacin from Water: Process Implications and Toxicological Evaluation. *J. Environ. Manage.* **2022**, *318*, No. 115515.

(36) Kusumawardani, C. The Calcination Effect on the Crystallinity, Nitrogen Content, and Pore Structure of Nitrogen-Doped Titanium Dioxide. *Jurnal Sains Dasar* **2022**, *11* (2), 118−125.

(37) Gadge, A. S.; Janbandhu, S. Y.; Sukhadeve, G. K.; Kumar, R.; Gajbhiye, C. D.; Gedam, R. S. TiO2 Nanoparticles for Methylene Blue Dye Degradation: Effect of Calcination Temperature. *ECS J. Solid State Sci. Technol.* **2023**, *12* (8), No. 086004.

(38) Oliveira, T. G.; Guerra, Y.; Araujo-Barbosa, S.; Gusmão, S. B. S.; Lobo, A. O.; Silva-Filho, E. C.; Santos, F. E. P.; Peña-Garcia, R.; Viana, B. C. Titanate Nanotubes and Their Magnetic Properties: Effect of Ion Exchange and Calcination Temperature. *J. Mater. Res.* **2023**, *38* (5), 1332−1348.

(39) Kiteto, M. K.; Mecha, C. A. Insight into the Bouguer-Beer-Lambert Law: A Review. *Sustainable Chem. Eng.* **2024**, 567−587.

(40) Muniz, F. T. L.; Miranda, M. A. R.; dos Santos, C. M.; Sasaki, J. M. The Scherrer Equation and the Dynamical Theory of X-Ray Diffraction. *Acta Crystallogr., Sect. A: Found. Adv.* **2016**, *72* (3), 385−390.

(41) Pirjade, B. S.; Jadhav, S. D.; Shaikh, I. A.; Khan, S. A. Photocatalytic Degradation of Methylene Blue Dye by Using Different Nanoparticles. *J. Adv. Res. Micro Nano Eng.* **2024**, *17* (1), 1−17.

(42) Desch, N.; Rheindorf, A.; Fassbender, C.; Sloot, M.; Lake, M. Photocatalytic Degradation of Methylene Blue by Anatase TiO2 Coating. *Appl. Res.* **2024**, *3* (5), No. e202300081.

(43) Borhani, M. N.; Tavakoli, A.; Mollaei, A. M.; Borhani, T. N. Visible Light Photodegradation of Methylene Blue by Ionic Liquid Based TiO2/Fe3O4 Nanophotocatalysts. *Opt. Mater.* **2024**, *154*, No. 115627.

(44) Özçelik, G.; Çavuşoğlu, F. C.; Bayazit, Ş.; Aydinoğlu, Ş. Ö. Photocatalytic Degradation of Methylene Blue Using Cu2 -Modified Bimetallic Titanium-Based Metal Organic Framework (MIL-125) Photocatalyst with Enhanced Visible Light Activity. *Turk. J. Chem.* **2024**, *48* (5), 756−769.

(45) Oviedo, L. R.; Druzian, D. M.; Nora, L. D. D.; da Silva, W. L. Biosynthesis and Characterization of a Novel Supported Nanocatalyst for the Methylene Blue Dye Photodegradation: Machine Learning Modeling and Photocatalytic Activity. *Catal. Today* **2024**, *441*, No. 114888.

(46) Afsa, S.; Hamden, K.; Martin, P. A. L.; Mansour, H. B. Occurrence of 40 Pharmaceutically Active Compounds in Hospital and Urban Wastewaters and Their Contribution to Mahdia Coastal Seawater Contamination. *Environ. Sci. Pollut. Res.* **2020**, *27* (2), 1941−1955.

(47) Wu, J.; Han, Z.; Ma, X.; Su, M.; Hamidian, A. H.; Zhang, Y.; Yang, M. A Database on Antibiotics and Antibiotic Resistance in Wastewater and Solid Waste from Pharmaceutical Industry Based on a Systematic Review. *China CDC Weekly* **2025**, *7* (3), 92−100.

(48) Li, J.; Xu, H.-Y.; Wang, A.-G.; Zhang, F.-J.; Sun, D.-S.; Oh, W.-C. Crack-Free TiO2 Films Prepared by Adjusting Processing Parameters via Liquid Phase Deposition Technique. *J. Korean Ceram. Soc.* **2020**, *57* (2), 206−212.

(49) Keshari, A. K.; Choudhary, P.; Shukla, V. K. Precursor Induced Evolution in Single Anatase Phase Synthesis of TiO2 Nanoparticles for Water Treatment and Dye-Sensitized Solar Cell. *Phys. B* **2022**, *631*, No. 413716.

(50) Pawar, N.; Bhargava, A.; Dayal, S.; Kumar, C. S. Synthesis and Characterization of Pure Anatase Phase Nanocrystalline TiO2 Thin Film by Magnetron Sputtering Method. *AIP Conf. Proc.* **2016**, *1728* (1), No. 020561.

(51) Argüelles-Lucho, P.; Pérez-Cuapio, R.; Woo-Garcia, R. M.; García-González, L.; Pacio, M.; López-Huerta, F. TiO2 Synthesis Anatase Phase with The Sol-Gel Process at Room Temperature. *IOP Conf. Ser.: Mater. Sci. Eng.* **2020**, *908* (1), No. 012003.

(52) Odling, G.; Robertson, N. Why Is Anatase a Better Photocatalyst than Rutile? The Importance of Free Hydroxyl Radicals. *ChemSusChem* **2015**, *8* (11), 1838−1840.

(53) Sakar, M.; Prakash, R. M.; Do, T.-O. Insights into the TiO2-Based Photocatalytic Systems and Their Mechanisms. *Catalysts* **2019**, *9* (8), No. 680.

(54) Liu, Z.-Q.; Kong, L.-Y.; Fei, B.-L. Highly Efficient Catalytic Reduction of Organic Dyes, Cr (VI) and 4-Nitrophenol, and

Photocatalytic Degradation of MB by an Inorganic−Organic Hybrid Polyoxometalate. *Appl. Organomet. Chem.* **2024**, *38* (9), No. e7599.

(55) Zhang, W.; Jiang, T.; Li, N.; Zhao, S.; Zhao, Y. Enhanced Photocatalytic Degradation of Methyl Orange by Metal-Tio2 Nanoparticles. *ChemistrySelect* **2024**, *9* (32), No. e202401814.

(56) Mohrhusen, L.; Al-Shamery, K. Conversion of Alcohols on Stoichiometric and Reduced Rutile TiO2 (110): Point Defects Meet Bifunctionality in Oxide (Photo-)Chemistry. *Catal. Lett.* **2023**, *153* (2), 321−337.

(57) Abromaitis, V.; Oghenetejiro, O. A. M. A.; Sulciute, A.; Urniezaite, I.; Sinkeviciute, D.; Zmuidzinaviciene, N.; Jankunaite, D.; Dzingeleviciene, R.; Baranauskis, K.; Martuzevicius, D. TiO2 Nanotube Arrays Photocatalytic Ozonation for the Removal of Antibiotic Ciprofloxacin from the Effluent of a Domestic Wastewater Treatment Plant: Towards the Process Upscaling. *J. Water Process Eng.* **2024**, *63*, No. 105457.

(58) Bera, A.; Bullert, D.; Hasselbrink, E. Vibrational Sum Frequency Spectroscopy Study of Methanol Adsorption on Thin Film TiO2 at Ambient Pressure and Temperature. *J. Phys. Chem. C* **2020**, *124* (29), 16069−16075.

(59) Wu, L.; Wu, Z.; Li, F.; Wang, Z.; Zhang, Z.; Gong, X.-Q.; Huang, W. Surface Reconstruction-Induced Photocatalytic Methanol Reduction Reaction on a Rutile TiO2(001) Surface. *J. Phys. Chem. Lett.* **2024**, *15* (33), 8481−8486.

(60) Dahal, A.; Petrik, N. G.; Wu, Y.; Kimmel, G. A.; Gao, F.; Wang, Y.; Dohnálek, Z. Adsorption and Reaction of Methanol on Anatase TiO2(101) Single Crystals and Faceted Nanoparticles. *J. Phys. Chem. C* **2019**, *123* (39), 24133−24145.

(61) Kovačević, M.; Simić, M.; Živković, S.; Milović, M.; Stojadinović, L. T.; Relić, D.; Anićijević, D. V. Uncovering Metal-Decorated TiO2 Photocatalysts for Ciprofloxacin Degradation—A Combined Experimental and DFT Study. *Int. J. Mol. Sci.* **2024**, *25* (21), No. 11844.

(62) Kaewkam, P.; Kanchanapaetnukul, A.; Khamyan, J.; Phadmanee, N.; Lin, K.-Y. A.; Kobwittaya, K.; Sirivithayapakorn, S. UV-Assisted TiO2 Photocatalytic Degradation of Virgin LDPE Films: Effect of UV-A, UV-C, and TiO2. *J. Environ. Chem. Eng.* **2022**, *10* (4), No. 108131.

(63) Tichonovas, M.; Krugly, E.; Jankunaite, D.; Racys, V.; Martuzevicius, D. Ozone-UV-Catalysis Based Advanced Oxidation Process for Wastewater Treatment. *Environ. Sci. Pollut. Res.* **2017**, *24* (21), 17584−17597.

(64) Joshi, S.; Kumari, A. Ozonation and Its Application in Wastewater Treatment *Int. J. Multidiscip. Res. Adv. Eng.* 2023; Vol. 5 6 DOI: 10.36948/ijfmr.2023.v05i06.8814.

(65) Pratiwi, W. Z.; Hadiyanto, H.; Widayat, W. Ozone-Based Advanced Oxidation Process for Pharmaceutical Contamination in Wastewater: A Review. *E3S Web Conf.* **2025**, *605*, No. 03058.

(66) Matsumi, Y.; Kawasaki, M. Photolysis of Atmospheric Ozone in the Ultraviolet Region. *Chem. Rev.* **2003**, *103* (12), 4767−4782.

(67) Touati, H.; Mehri, A.; Karouia, F.; Richard, F.; Batiot-Dupeyrat, C.; Daniele, S.; Clacens, J.-M. Low-Temperature O3 Decomposition over Pd-TiO2 Hybrid Catalysts. *Catalysts* **2022**, *12* (4), No. 448.

(68) Liu, S.; Zhai, G.; Zhang, H.; Si, S.; Liu, Y.; Mao, Y.; Wang, Z.; Cheng, H.; Wang, P.; Zheng, Z.; Dai, Y.; Huang, B. Enhanced Photocatalytic Ozonation Using Modified TiO2 With Designed Nucleophilic and Electrophilic Sites. *Chem. − Eur. J.* **2024**, *30* (51), No. e202401380.

(69) Li, X.; Wei, H.; Song, T.; Lu, H.; Wang, X. A Review of the Photocatalytic Degradation of Organic Pollutants in Water by Modified TiO2. *Water Sci. Technol.* **2023**, *88* (6), 1495−1507.

(70) Wu, L.; Wu, Z.; Wang, Z.; Xu, H.; Chai, P.; Huang, W. In Situ Generated Ti3+-Mediated Photocatalytic Methanol Decomposition to Carbon Monoxide and Hydrogen on a Rutile TiO2(100) Surface. *J. Phys. Chem. Lett.* **2022**, *13* (11), 2614−2618.

(71) Thammaacheep, P.; Suriwong, T.; Jannoey, P.; Khanitchaidecha, W.; Nakaruk, A.; Channei, D. Bio-Synthesis of TiO2 Photocatalyst: A Reduced Step Approach Using Leaf Extract. *Green Chem. Lett. Rev.* **2024**, *17* (1), No. 2433607.

(72) Constantin, M. A.; Constantin, L. A.; Ionescu, I. A.; Nicolescu, C. M.; Bumbac, M.; Tiron, O. Performance of a Solar Driven Photocatalytic Membrane Reactor for Municipal Wastewater Treatment. *Processes* **2024**, *12*, No. 617, DOI: 10.20944/preprints202402.0608.v1.

(73) Tang, Q.; He, J.; Fu, Q.; Zhao, L.; Tang, H.; Xie, L.; Liu, C.; Jiang, L.; Wang, J. Enhanced Photocatalytic Degradation Performance of Cornstalk Templated TiO2 towards Ciprofloxacin in Hospital Wastewater by the Synergistic Effect of the (101)/(001) Facets Coexposed and NiO Cocatalyst. *J. Alloys Compd.* **2024**, *992*, No. 174503.

(74) Nair, N.; Gandhi, V.; Shukla, A.; Ghotekar, S.; Nguyen, V.-H.; Varma, K. Mechanisms in the Photocatalytic Breakdown of Persistent Pharmaceutical and Pesticide Molecules over TiO2-Based Photocatalysts: A Review. *J. Phys.: Condens. Matter* **2024**, *36* (41), No. 413003.

(75) Noroozi, R.; Gholami, M.; Oskoei, V.; Arani, M. H.; Mousavifard, S. A.; Le, B. N.; Fattahi, M. Fabrication of New Composite NCuTiO2/CQD for Photocatalytic Degradation of Ciprofloxacin and Pharmaceutical Wastewater Treatment: Degradation Pathway, Toxicity Assessment. *Sci. Rep.* **2023**, *13* (1), No. 16287.

(76) Liu, Y.; Kamali, M.; Chen, X.; Rossi, B.; Appels, L.; Dewil, R. Photocatalytic Defluorination of Ciprofloxacin by Nitrogen-Defected g-C3N4 under Simulated Sunlight: Mechanistic Insight and Pathway Analysis. *Chem. Eng. J.* **2024**, *493*, No. 151950.

(77) Usman, M. R.; Prasasti, A.; Islamiah, S.; Firdaus, A. N.; Marita, A. W.; Fajriyah, S.; Noviyanti, A. R.; Eddy, D. R. Degradation of Ciprofloxacin by Titanium Dioxide (TiO2) Nanoparticles: Optimization of Conditions, Toxicity, and Degradation Pathway. *Bull. Chem. React. Eng. Catal.* **2021**, *16* (4), 752−762.

(78) Arlos, M. J.; Liang, R.; Fong, L. C. M. L. C.; Zhou, N. Y.; Ptacek, C. J.; Andrews, S. A.; Servos, M. R. Influence of Methanol When Used as a Water-Miscible Carrier of Pharmaceuticals in TiO2 Photocatalytic Degradation Experiments. *J. Environ. Chem. Eng.* **2017**, *5* (5), 4497−4504.

(79) Triquet, T.; Tendero, C.; Latapie, L.; Manero, M.-H.; Richard, R.; Andriantsiferana, C. TiO2MOCVD Coating for Photocatalytic Degradation of Ciprofloxacin Using 365 Nm UV LEDs - Kinetics and Mechanisms. *J. Environ. Chem. Eng.* **2020**, *8* (6), No. 104544.